Autonomous Raman Amplifiers in Software-Defined Optical Transport Networks

Autonomous Raman Amplifiers in Software-Defined Optical Transport Networks

Giacomo Borraccini*[(1)], Stefano Straullu[(2)], Alessio Ferrari[(1)],
Stefano Piciaccia[(3)], Gabriele Galimberti[(3)], Alberto Tanzi[(3)], Vittorio Curri[(1)]

[(1)] *Politecnico di Torino, Turin, Italy;* [(2)] *LINKS foundation, Turin, Italy;* [(3)] *Cisco Photonics, Vimercate, Italy*
**giacomo.borraccini@polito.it*

***Abstract*—Within a context of software-defined optical transport networks (SD-OTN), this work addresses specifically the management of Raman amplification, aiming to introduce and experimentally validate a system able to autonomously control this feature *in-situ*. In particular, given the required amplification constraints, an ad-hoc software module has been developed in order to optimize Raman pump power levels. Then, relaying on this software, the architecture of an embedded controller to install on board the Raman card has been defined to handle Raman pumps. The use of a conceived probing procedure allows to self-adapt each Raman amplifier to the installed fiber, allowing it to autonomously operate at the working point required by the control plane. Relying on the system telemetry, the proposed architecture controls the Raman pumps in order to achieve the required amplification constraints in terms of average gain and tilt. The entire proposal is validated through a set of experimental measurements that proofs both the achievement of the required gain target and the importance of the probing phase procedure in making the Raman amplifier autonomous and self-adaptable.**

***Index Terms*—Raman amplification, software-defined optical networks, optical fiber**

I. Introduction

Nowadays, the Raman amplification is a well established technique in optical transport networks (OTNs) enabling higher-capacity, longer reaches and and multi-band transmission [1], [2]. Its usage within optical communication systems is due to the multiple benefits that derive from it. In particular, Raman amplification allows to massively exploit the capacity of fiber links, by enabling the enlargement of the number of available channels [3], [4]. Moreover, Raman amplification systems exhibit a lower equivalent noise figure with respect to systems based on Erbium-doped fiber amplified (EDFA) only [5], [6]. As a consequence, this technique is extremely promoted and encouraged in long-haul optical transmissions [7], [8]. Designs for highly performative amplification systems adopt Erbium-doped Raman amplifiers (EDRAs) which combine the effects of the two techniques in order to reach the trade-off in terms of spectral occupancy, maximum reach and noise degradation [9]. In previous works [10]–[12], Raman amplification issue has been firstly addressed in optical communications in order to solve the mathematical question related to the optimization of amplification constraints. Machine-learning (ML) techniques have been effectively applied to Raman amplification [13], [14], but requiring a large training data-set. Regarding its use in optical networks, software-defined networks (SDNs) extensively adopt Raman amplification for controlling high-capacity and long-haul connections [15]–[17]. In particular, the authors have illustrated and validated a controller architecture able to locally manage Raman amplification in a SDN context [18]. In this perspective, the aim of this work is to introduce the description of a system able to fully lead the autonomous management of this feature *in-situ*. The controller architecture is contextualized within an optical network orchestrated by the control plane, explaining the operating behavior of the developed software modules. To fully automatize Raman amplifiers, an ad-hoc probing procedure is presented, allowing them to acquire the needed knowledge regarding the physical layer in which are introduced. As proof of concept, an experimental setup has been developed and analyzed to emulate the conceived system, and experimental results on different working points are shown. The presented approach is purely analytical. On the contrary of ML, the main advantage given by this proposal is the acquisition of the physical layer information through a fast probing procedure, avoiding long *a-priori* data-set acquisitions. Furthermore, thanks to the conceived architecture, the operating behavior is extremely flexible with respect to in-field modifications, which is not so feasible for ML approaches.

II. Controller Architecture and Network Integration

In this section, we describe the conceived controller architecture for an embedded system able to autonomously handle Raman amplification for each fiber span within an optical line system, bringing out the role of every software part and

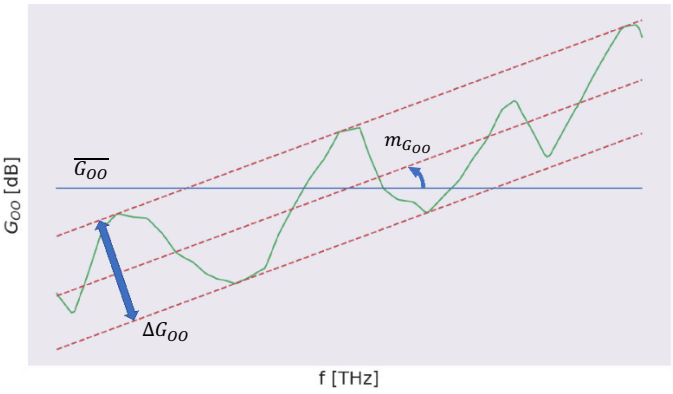

Fig. 1. Metrics of interest in the on-off gain profile G_{OO}.

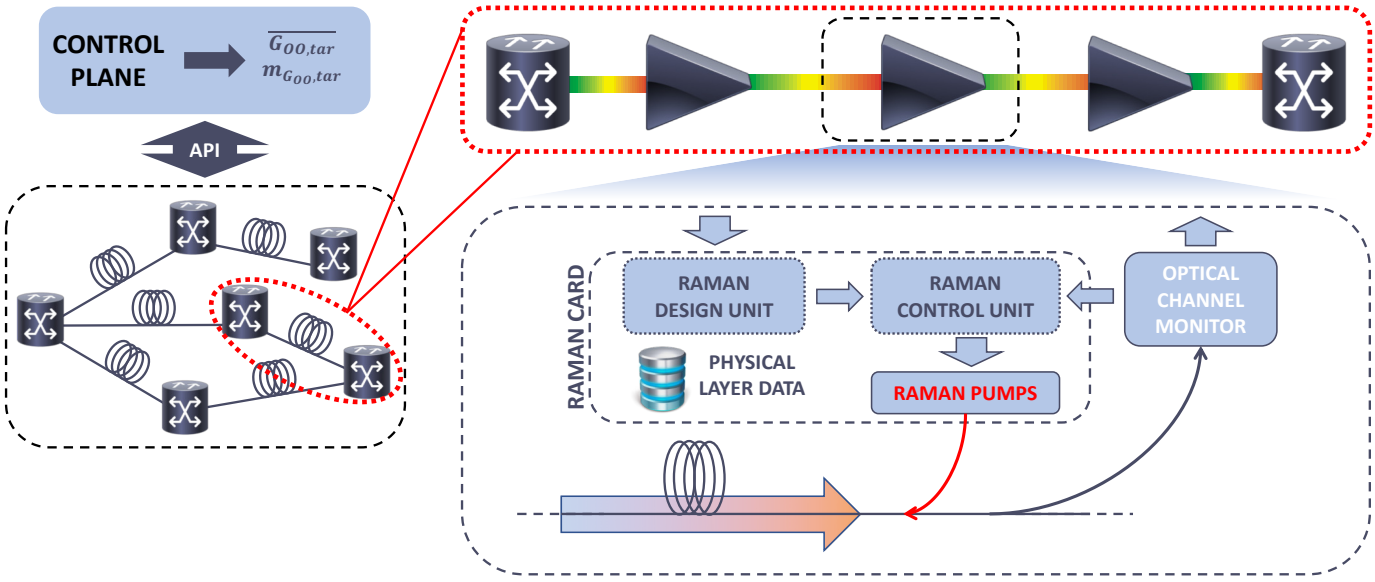

Fig. 2. Embedded controller architecture for Raman amplification and network integration.

contextualizing their interaction in a software-defined optical transport network (SD-OTN).

In order to fully understand the meaning of autonomous management of Raman amplification, it is important to define the metrics of the optimization process. A generic on-off gain profile G_{OO} is represented in Fig. 1. The Raman amplification optimizer is based on the evaluation of the average on-off gain $\overline{G_{OO}}$, the slope of the linear regression $m_{G_{OO}}$, and the maximum deviation from the linear regression ΔG_{OO}.

The proposed embedded controller architecture for Raman amplification and its network contextualization are illustrated in Fig. 2. Each Raman card has an on board software module constituted by two units: the Raman Design Unit (RDU) and the Raman Control Unit (RCU). The RDU is responsible for defining the optimal working point of the Raman amplification site, determining power configuration of Raman pumps that matches the requested amplification mask. On the other hand, the RCU is in charge of setting Raman pumps and tracking the mean gain in case of spectral load variations or scenario modifications.

Once the optical network is installed, the first step before deploying wavelength division multiplexing (WDM) optical transport is the calibration of each Raman amplifier by means of a probing procedure. This phase, described in detail in next section, is needed to acquire the physical layer knowledge for feeding the RDU optimization framework. The effective operation starts computing the working point of each network amplification site by the control plane and the consecutive configuration of the amplification constraints in terms of mean gain $\overline{G_{OO,tar}}$ and tilt $m_{G_{OO},tar}$ of each Raman amplifier. Locally, every Raman card receives the target information and sets the relative target gain-mask. Relying on the physical layer information, the RDU defines the Raman pump configuration that maximizes the match between the amplification constraints and the real gain features. The optimization procedure is done regardless of the channel spectral load, taking into account only inter-pump effects. Then, the Raman pump power configuration is computed by the RCU that consequently sets the Raman pumps. Thanks to a linearization algorithm based on the evaluation of power gradients with respect to the gain variation, the RCU controls the Raman pumps in order to achieve the mean gain, exploiting telemetry data provided by optical channel monitors (OCMs).

Analysing the execution time for a single fiber span, the RDU optimization process needs a time interval that goes from 4 to 20 minutes, considering a very large casuistry of in-field emulations done by means of the developed framework. This operation is time-consuming but it needs to be performed just once at the beginning of the operative phase of the system, and can be done simultaneously for every amplifying site as it is a local procedure. When the optimal Raman configuration is set, the RCU performs simple analytical computations in order to adjust the mean gain towards the gain target with real-time response.

Main advantages delivered by the proposed controller architecture concern the adaptability with respect to optical specific link features and the high degree of flexibility with respect to spectral load variations. In particular, the conceived probing procedure and the controller structure allow to easily manage scenario modifications as fiber cuts or components' aging. Moreover, the general description of the optimization problem allows to control both multi-band and single-band transmission according to the network request.

III. Probing Phase Description

In this section, the description of the initial probing phase for acquiring the physical layer data is presented. This step is performed for each Raman amplifier on the optical line system

before starting the normal operation. This is fundamental in order to make the system aware of the physical characteristics of the fiber link and to properly adjust the working point of the Raman amplifier in case of lack of knowledge in the physical domain.

As premises, Raman pumps have to be previously calibrated in order to introduce into the fiber the desired optical power. The non-flat frequency response of the optical devices along the link must be carefully characterized and taken into account. The software module on board of each Raman amplifier needs the following unknown physical parameters to correctly perform computations:

- the lumped losses along the fiber span $l_c(z)$;
- the Raman efficiency of the fiber $C_r(\Delta f)$;
- the loss coefficient function $\alpha(f)$;
- the correction parameters $\overline{G_{OO,cor}}$, $m_{G_{OO},cor}$.

The probing procedure we are illustrating has been conceived to let the system operate in the largest possible number of scenarios without making its application too complex or too long. To do this, we adopt some simplifications about the acquisition of the Raman efficiency. In particular, the shape of the Raman efficiency profile is assumed known and only the scaling factor of this curve is probed [19]. In practice, this approximation is supported by characterization of different fiber types, available in literature [1] as the frequency variation of the Raman efficiency for different fiber types is similar. The Raman efficiency is rewritten in the following form:

$$C_r(\Delta f) = K_r \, c_r(\Delta f) \, , \tag{1}$$

where K_r is the Raman efficiency scaling factor expressed in $(m \cdot W)^{-1}$ and c_r is the normalized Raman efficiency curve, containing the shape information.

The probing procedure is articulated in five different steps that aim to extract *1)* the lumped losses along the fiber $l_c(z)$, *2)* the loss coefficient function for the pump frequencies $\alpha(f_p)$, *3)* the Raman efficiency scaling factor K_r, *4)* the loss coefficient function for channel frequencies $\alpha(f_{ch})$ and *5)* the correction parameters.

1) OTDR Analysis: Firstly, an analysis of the fiber link is made through optical time domain reflectometer (OTDR). This allows to detect concentrated losses l_c, such as splices, connectors and non-idealities. This step is not mandatory: if the OTDR is not available, lumped losses will be taken into account within the loss coefficient function of the fiber as a distributed effect.

2) Measurements with back-reflection photodiode: By means of the back-reflection photodiode (BRP) at the transmitter side, the loss coefficient function is evaluated at the Raman pump frequencies. This probing step is done performing a measurement for each Raman pump (with WDM channels turned off). Considering logarithmic units, the loss coefficient function for pump frequencies is calculated as follows:

$$\alpha(f_p) = \frac{P(f_p, L_S) - P(f_p, 0) + \sum l_c(z)}{L_S} \, , \tag{2}$$

where $P(f_p, L_S)$ is the pump launch power, $P(f_p, 0)$ is the power detected by the BRP, $\sum l_c(z)$ is the sum of the concentrated loss and L_S is the fiber span length.

3) Pump&Probe Measurements: To extract the Raman efficiency scaling factor K_r, a set of pump & probe (P&P) measurements is performed. For each Raman pump, the measurement is done using, as a probe, the channel that maximizes the Raman coupling, so that $\Delta f \approx 13$ THz. Therefore, the on-off gain on the probe G_{OO} is computed from the P&P measurement. As the P&P involves one single channel, it is reasonable to assume undepleted pump [20] and so Raman efficiency can be extracted from the following equation [21]:

$$C_r(f_p - f_{ch}) = \frac{ln(G_{OO}(f_{ch}))}{L_{eff}(f_p) P(f_p, L_S)} \, , \tag{3}$$

where $L_{eff}(f_p)$ is the fiber effective length at the pump frequency:

$$L_{eff}(f_p) = \frac{1 - e^{-\alpha(f_p) L_S}}{\alpha(f_p)} \, . \tag{4}$$

From Eq. 1, the Raman efficiency scaling factor is obtained for each Raman pump. Lastly, the K_r is estimated by averaging the computed values.

4) Complete WDM Spectrum Propagation: This step allows to analytically compute the loss coefficient function for channel frequencies $\alpha(f_{ch})$ and it is done with Raman pumps turned off. In particular, the algorithm consists in:

- propagation of the full WDM spectrum along the fiber span;
- acquisition of the power spectra at transmitter $P_{off}(f, 0)$ and receiver $P_{off}(f, L_S)$ sides through OCMs;
- computation of the tilt of the received spectrum m_{P_s} as the slope of its linear regression;
- the estimation of the average loss coefficient $\overline{\alpha}$ by means of the following formula:

$$\overline{\alpha} = \overline{\left(\frac{P_{off}(f, 0) - (P_{off}(f, L_S) + \sum l_c(z))}{L_S} \right)} \, ; \tag{5}$$

- emulation of the system introducing the average loss coefficient function $\overline{\alpha}$ and the extracted Raman efficiency profile;
- computation of the power difference $\Delta P(f)$ between the effective received spectrum $P_{off}(f, L_S)$ and the emulated one $P_{off}^{EMU}(f, L_S)$ (dBm):

$$\Delta P(f) = P_{off}(f, L_S) - P_{off}^{EMU}(f, L_S) \, ; \tag{6}$$

- extraction of the loss coefficient function $\alpha(f)$ through the following formula:

$$\alpha(f) = \left(\frac{\Delta P(f)}{P_{off}(f, L_S)} + 1 \right) \overline{\alpha} \, . \tag{7}$$

Eq. 7 refers to the extraction of the loss coefficient vs. frequency, starting from the difference between experimental results and emulation done with flat loss coefficient (Eq. 6). Thus, the optimization frame collects information about fiber attenuation, separating the tilt contributions of the fiber loss from the Raman cross-talk effect.

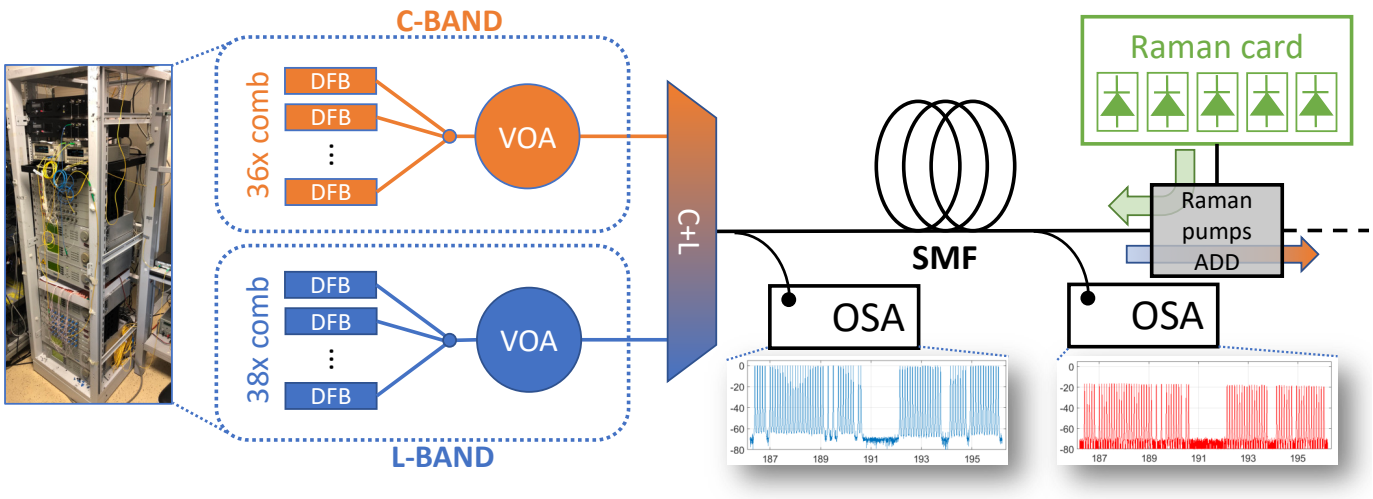

Fig. 3. Experimental equipment.

5) Optimization at Maximum Gain: In order to finalize the probing procedure, a first Raman amplification optimization is performed at the maximum gain target $\overline{G_{tar,MAX}}$ achievable by the system on the WDM spectrum. After the optimization, mean on-off gain $\overline{G_{OO}}$ and tilt $m_{G_{OO}}$ are extracted from telemetry. These data are compared with target values, and correction parameters are computed:

$$\overline{G_{OO,cor}} = \overline{G_{OO,tar,MAX}} - \overline{G_{OO}} \ , \tag{8}$$

$$m_{G_{OO},cor} = m_{G_{OO},tar} + m_{G_{OO}} \ . \tag{9}$$

Generally, $m_{G_{OO},tar}$ is set to 0 because the purpose of the optimization is to restore the flatness of the WDM spectrum. The aim of this final probing step is to center the virtual gain mask produced by the optimization framework in the correct working point, in order to fill the lack of knowledge and to compensate for any uncertainty.

IV. Experimental Results

In order to verify the behavior of the entire controller architecture and to validate the effectiveness of the probing procedure, an experimental campaign has been fulfilled. In this section, the experimental equipment is firstly described. Then, the probing phase results are shown and commented in order to remark the meaning of the performed steps. Finally, the experimental results proving the operative behavior of the conceived Raman amplifier under different working points are reported.

A. Experimental Setup

The experimental equipment is sketched in Fig. 3. A comb of distributed feedback (DFB) lasers composes the input WDM spectrum. By using a continuous-wave (CW) comb we do not lose in generality, as Raman gain is not sensible to the signal modulation but only to the average power level. In particular, two input WDM spectra are created in L-band (38 channels) and C-band (36 channels), and the final WDM spectrum is generated using a C+L coupler. The introduction of variable optical attenuators (VOA) allows to rigidly modify C and L input spectrum powers. Connecting two standard single mode fiber (SSMF) spools of 60 km and 25 km nominal lengths, a fiber span link of 85 km nominal length is built.

At the receiver side, 5 counter-propagating Raman pumps with frequencies spread in [200 - 210] THz frequency range are introduced by means of an optical coupler. In order to emulate telemetry devices, an optical spectrum analyser (OSA) is used at both fiber span terminals.

B. Probing Phase Results

Tracing the steps of the proposed probing procedure, results achieved from the probing of the experimental equipment are shown.

The OTDR analysis carried out on the fiber span link is reported in Tab. I. Reasonably, there are two insertion losses placed at both fiber span terminals due to the input connector and the output splitter and an intermediate lumped loss due to fiber spools connector.

Prosecuting with the extraction of the scaling factor for Raman efficiency, results are shown in Fig. 4. Following the loss coefficient function at pump frequencies $\alpha(f_p)$, the P&P measurements accurately estimate the strength of the Raman amplification coupling, comparing the extracted value with respect to the theoretical one.

The algorithmic steps for channel loss coefficient function $\alpha(f_{ch})$ are depicted in Fig. 5. This picture clearly expresses

TABLE I
Lumped Losses

Loss Intensity	Loss Position
0.2 dB	0 km
0.18 dB	61.006 km
0.3 dB	86.081 km

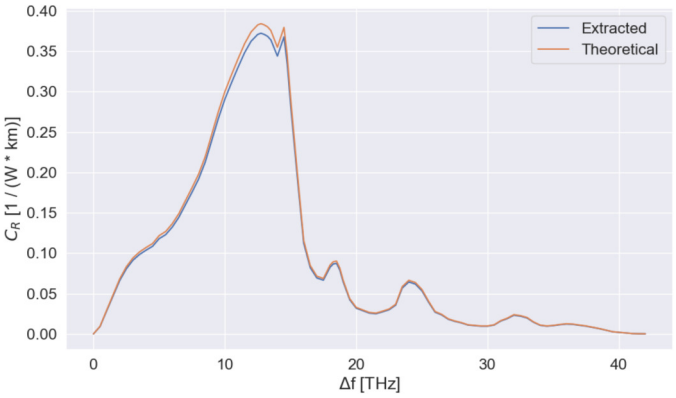

Fig. 4. Extracted Raman efficiency profile.

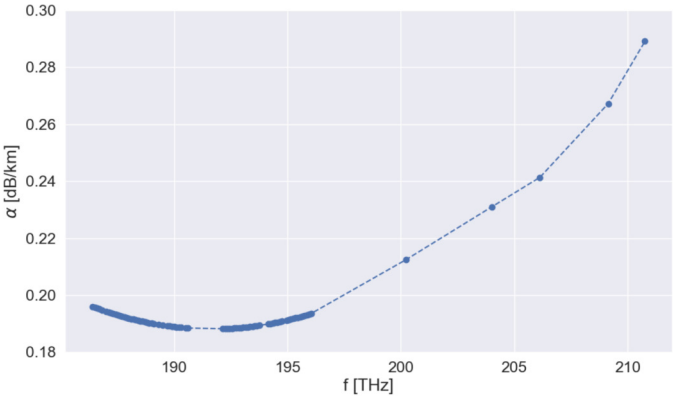

Fig. 6. Extracted loss coefficient function.

the mathematical meaning of Eq. 7: starting from the flat average loss coefficient function $\overline{\alpha}$ (light blue straight line), the frequency content (red square markers) is extracted by exploiting the power difference $\Delta P(f_{ch}, L_S)$ between the real received spectrum and the received one emulated using the average $\overline{\alpha}$. In order to smooth the profile trend, the extracted curve undergoes a polynomial second order fitting (blue circle markers). The final result that summarizes the complete extracted loss coefficient function $\alpha(f)$, considering both channels and pumps, is reported in Fig. 6.

C. Measurement Results

After the probing phase, a set of measurements is carried out to verify that the conceived Raman controller architecture works correctly.

Firstly, the WDM spectrum is acquired with Raman pumps turned off (Fig. 7). Having an almost flat input WDM spectrum around 0 dBm per channel, this measurement allows to capture the information regarding the output WDM spectrum tilt m_{P_S}, useful to emulate amplification constraint on gain tilt. So, by defining the tilt target $m_{G_{OO}}$ to 0.2774 dB/THz, three different requests by control plane on amplification are tested, requiring gain targets $\overline{G_{OO}}$ of 8, 9 and 10 dB. These values for gain target are chosen because they are challenging Raman requests that recover for more than half of the fiber loss.

Provided the amplification constraints to the Raman software module, the system starts computing the optimal Raman pump power configuration. Subsequently, it sets the Raman pumps at the set working point and tries to achieve the gain target within a tolerance of a tenth of dB, linearizing the problem around the optimum working point. The achieved Raman pump power configurations are reported in Tab. II. The complete set of experimental results is illustrated in Figs. 8, 9. Fig.8 displays as the gain target has been successfully obtained with the required tolerance range for each test scenario. On the other hand, by observing Fig. 9, also the required tilt is achieved in all cases. Only a residual negligible 0.2 dB tilt on 10 THz is observed. Regarding the ripple, the optimizer

TABLE II
RAMAN PUMP POWER CONFIGURATIONS

$\overline{G_{OO,tar}}$ [dB]	$P_{P,1}$ [mW]	$P_{P,2}$ [mW]	$P_{P,3}$ [mW]	$P_{P,4}$ [mW]	$P_{P,5}$ [mW]
8	198.5	150.0	133.5	39.3	91.7
9	224.4	177.0	148.3	42.9	95.1
10	241.2	212.8	164.5	46.2	100.9

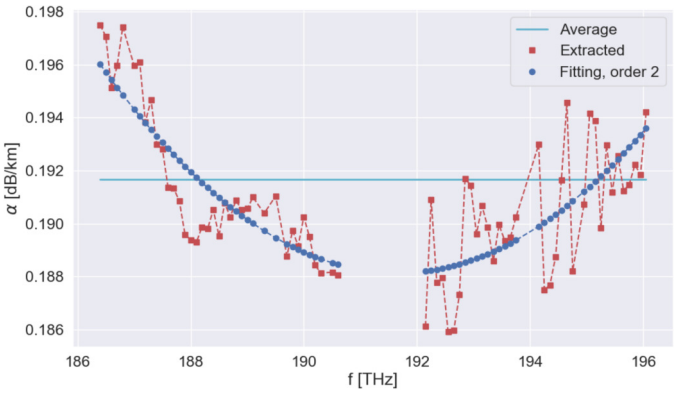

Fig. 5. Algorithmic steps for extracting loss coefficient function at channel frequencies $\alpha(f_{ch})$.

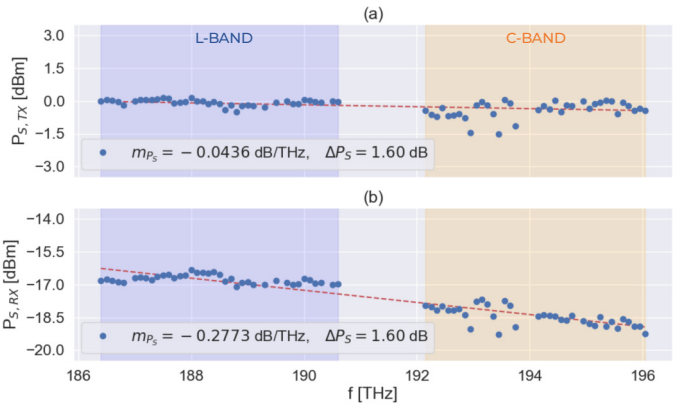

Fig. 7. Raman pumps off: (a) transmitted power spectrum, (b) received power spectrum.

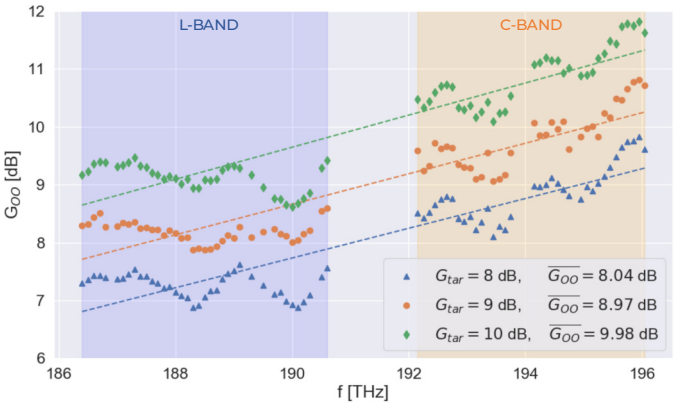

Fig. 8. Measured on-off gain profiles with relative metrics.

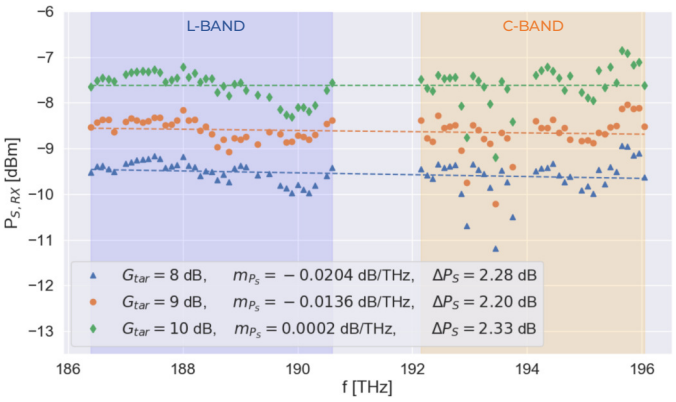

Fig. 9. Measured output WDM spectra with relative metrics.

aims at its minimization, but it cannot be completely removed due to the shape of Raman efficiency. In any case, this ripple increment is always kept below 1 dB.

V. Conclusion

In this work, we propose and experimentally validate an autonomous Raman amplifier architecture able to operate within a software-defined optical transport network. The operating behavior and the interaction between the actors of the optical line system have been illustrated, defining a probing procedure which enables the full physical layer awareness by each network Raman card. Moreover, the entire proposal is verified through a set of experimental measurements that shows the achievement of the required amplification constraints and justifies the role of the probing phase procedure in making the Raman amplifier autonomous and self-adaptable.

Acknowledgment

This work has been supported by Cisco Photonics within a SRA contract.

References

[1] J. Bromage, "Raman amplification for fiber communications systems," *Journal of Lightwave Technology*, vol. 22, no. 2, p. 79, 2004.

[2] M. N. Islam, "Raman amplifiers for telecommunications," *IEEE Journal of selected topics in Quantum Electronics*, vol. 8, no. 1, pp. 548–559, 2002.

[3] V. E. Perlin and H. G. Winful, "On distributed raman amplification for ultrabroad-band long-haul wdm systems," *Journal of lightwave technology*, vol. 20, no. 3, p. 409, 2002.

[4] S. Namiki and Y. Emori, "Ultrabroad-band raman amplifiers pumped and gain-equalized by wavelength-division-multiplexed high-power laser diodes," *IEEE Journal of Selected Topics in Quantum Electronics*, vol. 7, no. 1, pp. 3–16, 2001.

[5] V. Curri and A. Carena, "Merit of raman pumping in uniform and uncompensated links supporting nywdm transmission," *Journal of Lightwave Technology*, vol. 34, no. 2, pp. 554–565, 2015.

[6] V. Curri, "System advantages of raman amplifiers," *Proc. NFOEC 2000*, vol. 1, pp. 35–46, 2000.

[7] W. S. Pelouch, "Raman amplification: An enabling technology for long-haul coherent transmission systems," *Journal of Lightwave Technology*, vol. 34, no. 1, pp. 6–19, 2015.

[8] M. Tan, P. Rosa, S. T. Le, I. D. Phillips, and P. Harper, "Evaluation of 100g dp-qpsk long-haul transmission performance using second order co-pumped raman laser based amplification," *Optics express*, vol. 23, no. 17, pp. 22 181–22 189, 2015.

[9] A. Carena, V. Curri, and P. Poggiolini, "On the optimization of hybrid raman/erbium-doped fiber amplifiers," *IEEE Photonics Technology Letters*, vol. 13, no. 11, pp. 1170–1172, 2001.

[10] Y. Emori, K. Tanaka, and S. Namiki, "100 nm bandwidth flat-gain raman amplifiers pumped and gain-equalised by 12-wavelength-channel wdm laser diode unit," *Electronics Letters*, vol. 35, no. 16, pp. 1355–1356, 1999.

[11] V. E. Perlin and H. G. Winful, "Optimal design of flat-gain wide-band fiber raman amplifiers," *Journal of lightwave technology*, vol. 20, no. 2, p. 250, 2002.

[12] X. Liu and Y. Li, "Optimizing the bandwidth and noise performance of distributed multi-pump raman amplifiers," *Optics communications*, vol. 230, no. 4-6, pp. 425–431, 2004.

[13] D. Zibar, A. Ferrari, V. Curri, and A. Carena, "Machine learning-based raman amplifier design," in *Optical Fiber Communication Conference*. Optical Society of America, 2019, pp. M1J–1.

[14] D. Zibar, A. M. R. Brusin, U. C. Moura, V. Curri, and A. Carena, "Inverse system design using machine learning: the raman amplifier case," *Journal of Lightwave Technology*, 2019.

[15] T. J. Xia, H. Fevrier, T. Wang, and T. Morioka, "Introduction of spectrally and spatially flexible optical networks," *IEEE Communications Magazine*, vol. 53, no. 2, pp. 24–33, 2015.

[16] X. Zhao, V. Vusirikala, B. Koley, V. Kamalov, and T. Hofmeister, "The prospect of inter-data-center optical networks," *IEEE Communications Magazine*, vol. 51, no. 9, pp. 32–38, 2013.

[17] X. Zhao, V. Vusirikala, B. Koley, T. Hofmeister, V. Kamalov, and V. Dangui, "Optical transport sdn for high-capacity inter-datacenter networks," in *Photonics in Switching*. Optical Society of America, 2014, pp. PM3C–1.

[18] G. Borraccini, A. Ferrari, S. Straullu, A. Nespola, A. D'Amico, S. Piciaccia, G. Galimberti, A. Tanzi, S. Turolla, and V. Curri, "Softwarized and autonomous raman amplifiers in multi-band open optical networks," in *International IFIP Conference on Optical Network Design and Modeling*, 2020.

[19] J. Bromage, K. Rottwitt, and M. Lines, "A method to predict the raman gain spectra of germanosilicate fibers with arbitrary index profiles," *IEEE Photonics Technology Letters*, vol. 14, no. 1, pp. 24–26, 2002.

[20] M.-S. Kao and J. Wu, "Signal light amplification by stimulated raman scattering in an n-channel wdm optical fiber communication system," *Journal of lightwave Technology*, vol. 7, no. 9, pp. 1290–1299, 1989.

[21] E. Pincemin, D. Grot, L. Bathany, S. Gosselin, M. Joindot, S. Bordais, Y. Jaouen, and J.-M. Delavaux, "Raman gain efficiencies of modern terrestrial transmission fibers in s-, c-and l-band," in *Nonlinear Guided Waves and Their Applications*. Optical Society of America, 2002, p. NLTuC2.